GOSPODARKA SUROWCAMI MINERALNYMI – MINERAL RESOURCES MANAGEMENT

2025 Volume 41 Issue 3 Pages 45–71

DOI: 10.24425/gsm.2025.155338

IBNU MUNZIR[1], IRENA BRUNARSKA[2], AKMAL SAPUTNO[3], ANNA ROKICIŃSKA[4], SRI ADI WIDODO[5], IRZAL NUR NUR[6], MAREK MICHALIK[7]

The characteristics of saprolitic nickel ore from lateritic nickel deposit in the Mandiodo Area, North Konawe, Indonesia

Introduction

Lateritic nickel deposits are a valuable source of nickel, accounting for approximately 70% of the global nickel reserves (Wulandari et al. 2020). These deposits are formed through

✉ Corresponding Author: Ibnu Munzir; e-mail: ibnu.munzir@doctoral.uj.edu.pl

[1] Institute of Geological Sciences, Jagiellonian University, Kraków, Poland; ORCID iD: 0000-0003-1138-7362; e-mail: ibnu.munzir@doctoral.uj.edu.pl

[2] Institute of Geological Sciences, Jagiellonian University, Kraków, Poland; ORCID iD: 0000-0002-3366-0633; e-mail: irena.brunarska@uj.edu.pl

[3] Institute of Geological Sciences, Jagiellonian University, Kraków, Poland; Mining Engineering Department, Hasanuddin University, Indonesia; ORCID iD: 0009-0001-2451-6234; e-mail: akmal.saputno@doctoral.uj.edu.pl

[4] Faculty of Chemistry, Jagiellonian University, Kraków, Poland; ORCID iD: 0000-0001-8397-4422; e-mail: anna.rokicinska@uj.edu.pl

[5] Mining Engineering Department, Hasanuddin University, Indonesia; ORCID iD: 0000-0001-8613-9107; e-mail: srwd007@yahoo.com

[6] Mining Engineering Department, Hasanuddin University, Indonesia; e-mail: irzal.nur@eng.unhas.ac.id

[7] Institute of Geological Sciences, Jagiellonian University, Kraków, Poland;ORCID iD: 0000-0001-5033-2589; e-mail: marek.michalik@uj.edu.pl

lateralization, an alteration process that occurs in ultramafic rocks containing olivine, pyroxene, and serpentine, which undergo a weathering process. Lateritic nickel deposit formation is controlled by the bedrock type, topography, geological structure, organic material, and weathering intensity (Butt and Cluzel 2013). Lateritic nickel deposits are categorized into three deposit types according to the nickel host mineral:

- the oxide type characterized by the domination of Fe-OxOH,
- the clay-silicate type identified by smectite-group mineral as a host of Ni, and
- the hydrous-silicate type indicated by domination of Mg-Ni phyllosilicates in the ore minerals (Brand et al. 1998; Freyssinet et al. 2005).

The humid tropical climate and active tectonic collisional zones are renowned for the occurrence of nickel laterite deposits, including those found in Indonesia, New Caledonia, Cuba, and the Philippines. Some deposits also occur in Brazil, Western Africa, and Australia in cratonic areas (Elias 2002). Southeast Sulawesi is categorized as a geological province of ultramafic rock that extends to the east of Sulawesi Island and is known as the East Sulawesi Ophiolite Belt (Kadarusman et al. 2004). Mandiodo is situated in the North Konawe region of Southeast Sulawesi Province, where, geologically, the area is composed of peridotite in the form of lherzolite, dunite, and harzburgite from the East Sulawesi Ophiolite (Kadarusman et al. 2004).

The development of nickel enrichment in lateritic deposits is influenced by the degree of serpentinization of Ni-rich bedrock (Irfan et al. 2021). Dublet et al. (2015) divided the lateritic nickel deposit into two main layers: a silicate-rich layer and an oxide-rich layer. The silicate-enriched layer, known as saprolite, comprises predominantly Mg- and Ni-bearing phyllosilicates like serpentine and, to a lesser degree, talc, and smectite. Additionally, it contains varying quantities of residual silicates, including olivine and pyroxene. The oxide-rich layer is characterized by the prevalence of Ni-bearing Fe-oxyhydroxides, primarily goethite, with minor quantities of hematite and maghemite. In certain instances, it is accompanied by Ni-Co-bearing manganese oxides, such as lithiophorite and asbolane (Soh Tamehe et al. 2024). Observing the characteristics of the saprolite horizon, including the element distribution, is important due to the source of the nickel ore in the lateritic deposit, mainly from this horizon. This study investigates the elements' distribution and the characteristics of the saprolite horizon as a primary source of lateritic nickel ore in the Mandiodo area.

1. Location and geological setting

There has been a growing interest in lateritic nickel deposits within the economic geology and exploration communities over the past two decades. This heightened attention is primarily attributed to advancements in metallurgical technology for processing lateritic nickel ores and the increasing scarcity of sulfide nickel resources.

The nickel deposit type in the study area is recognized as a lateritic nickel deposit developed on ultramafic rocks from the weathering of ultramafic rock from the East Sulawesi Ophiolite (Figure 1). The East Sulawesi Ophiolite Belt is a member of the multiple

ophiolite belts of the Circum Pacific Phanerozoic formed from the Cretaceous to Miocene periods by convergent plate processes (Hall and Wilson 2000). This ophiolite, dominated by peridotite, is tectonically dismembered and cropped out over 10,000 km^2 in eastern Sulawesi (Monnier et al. 1995). After investigating the mineralogy of lateritic nickel ore from East Sulawesi, Fu et al. (2014) explained that the lateritic nickel deposit is mainly composed of red soil, limonite zone, saprolite horizon, and bedrock. The silicate mineral formed after the alteration process mainly consists of serpentine, while Fe-oxyhydroxides are dominated by goethite in the laterite profile from the weathering process. From the bedrock to the red soil,

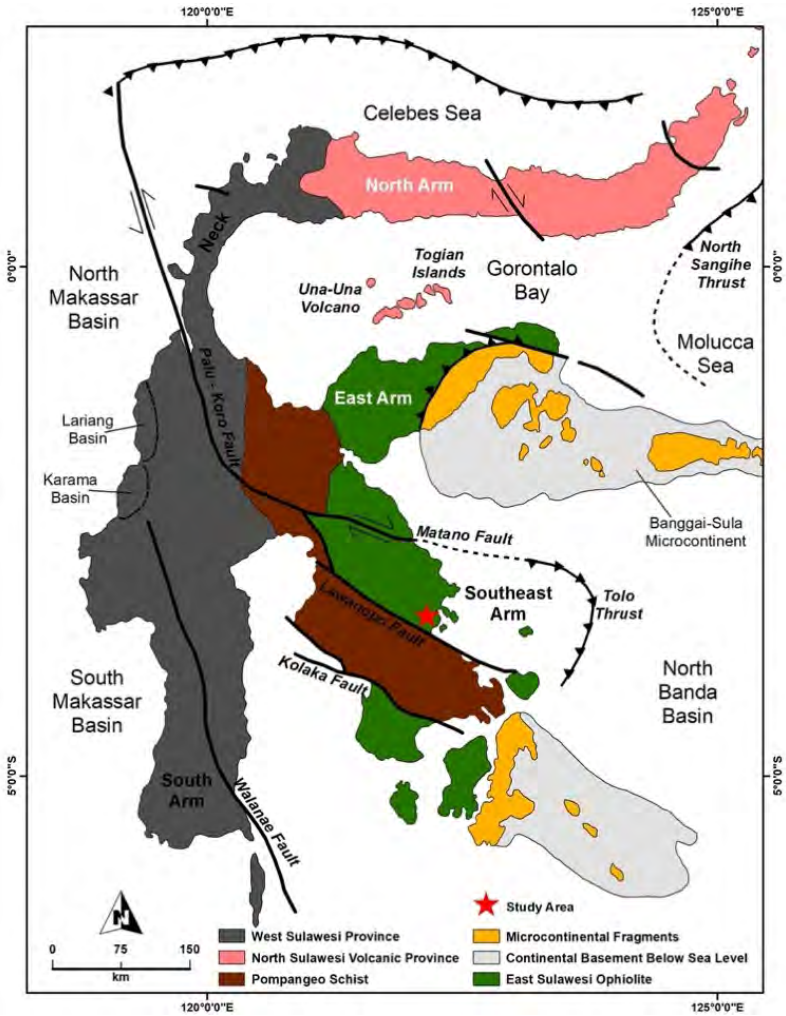

Fig. 1. The geological map of Sulawesi showing the distribution of East Sulawesi Ophiolite (modified after White et al. 2014) and the location of the study area (red star)

Rys. 1. Mapa geologiczna Sulawesi przedstawiająca rozmieszczenie ofiolitu z Sulawesi Wschodniego oraz lokalizację obszaru badań (czerwona gwiazdka)

the Si and Mg concentrations gradually depleted, while the Fe, Al, and Cr gradually enriched, and the highest Ni concentrations (11.53% NiO) were found in the saprolite horizon (Zhang et al. 2020).

Kadarusman et al. (2004) examined the geochemistry of East Sulawesi, discovering that ophiolite is extensively found throughout East-Central Sulawesi, extending from north to south over approximately 700 km and covering more than 15,000 km^2 of outcrops. They observed the transition from peridotite in the bedrock layer to isotropic gabbro, followed by sheeted dolerites and basalt volcanic rocks in the upper part of the deposit. The oxidized peridotite primarily consists of spinel lherzolite, with harzburgite and dunite intercalation. Notably, there are significant variations in the mineral composition between different horizons, resulting in substantial differences in the content of Mg-Fe-Si across different regions.

The lateritic nickel deposits' weathering crusts are divided by the residual laterite horizon, the rotten rock horizon ("saprock"), and the bedrock horizon (Parkinson 1998; Hall and Wilson 2000). The study area features an undulating landscape of low to moderate elevation changes. Under this condition, the lateritic profile results from the chemical weathering of exposed ultramafic rock.

2. Materials and methods

The lateritic profile in the study area is divided into six different horizons based on their characteristics: topsoil, transition zone, limonite zone, saprolite, saprock, and bedrock (Figure 2).

The topsoil layer ranges from dark reddish-brown to very dark brown and is compact in several parts due to the presence of ferricrete. The layer consists mainly of iron oxides, including goethite, hematite, and magnetite. The transition zone appears in a brighter color compared to the topsoil and limonite zones, with the domination of the gibbsite influenced by the higher concentration of aluminum. The limonite zone is characterized by the dark reddish-brown color with the domination of limonite minerals. The saprolite horizon and saprock horizon are almost similar in color, ranging from strong brown to greenish-pale yellow. However, the saprock contains a considerable amount of large rock fragments. Lastly, the bedrock appears to be a light grey to dark green color, very hard and compact, with a massive structure. The bedrock consists mainly of olivine, pyroxene, and serpentine minerals. During the sample collections, the garnierite is rarely found along the lateritic profile.

2.1. Sample collection and preparation

Twelve samples analyzed in the study were collected vertically from the whole lateritic profile from bedrock to topsoil horizon in an open pit mine at the Mandiodo area aimed for

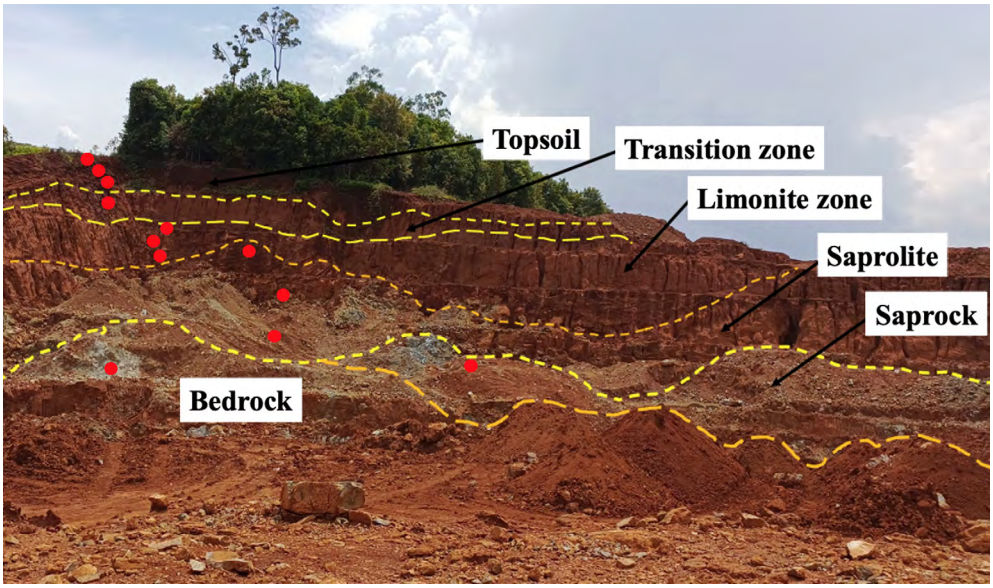

Fig. 2. The sampling location in the Mandiodo site divided into topsoil, limonite, saprolite, and bedrock. The Sampling spots are marked in red dot

Rys. 2. Miejsce poboru próbek w miejscu Mandiodo podzielone na wierzchnią warstwę gleby, limonit, saprolit i podłoże skalne.
Miejsca poboru próbek zaznaczono czerwonymi kropkami.

several different analyses (Figure 2). The samples were prepared in polished thin sections and powdered samples for further analyses. Homogenization was conducted prior to preparation to obtain representative powdered samples. The collected samples were dried at 50°C using an oven for 24 hours to reduce their moisture content before being reduced in grain size to 74 microns using an agate mortar and sieve. The size is expected to meet the requirements for the mineralogical and chemical analyses. The samples were also prepared in polished thin section samples for petrography and mineral chemistry analyses.

2.2. Optical microscope

Five polished thin section samples from bedrock to saprolite were observed using an optical microscope equipped with a UV Fluorescence Nikon Eclipse Ni polarising microscope and Lumen 200 UV system lighting, staged with a Proscan Prior drive, Nikon DS Fi 1C digital camera, Nikon Digital Sight DS-U3 camera controller, and an HP Z440 graphics PC workstation. The purpose of the analysis was to recognize the petrology of the taken samples from the study area.

2.3. XRF (X-ray fluorescence)

To obtain the geochemical characteristics of the samples, the 12 powdered samples from whole layers were analyzed with the X-ray fluorescence (XRF) technique using the EDXRF ARL QUANT'X spectrometer (Thermo Scientific) conducted at the Department of Chemical Technology, Faculty of Chemistry, Jagiellonian University in Kraków, Poland. The analysis shows the geochemical characteristics of the samples from the study area, including the elements' distribution from the bedrock to saprolite horizon.

2.4. XRD (X-ray diffraction)

To identify the main compounds and phases present in the samples, including their mineralogical characteristics, powder X-ray diffraction (XRD) analysis was carried out using a Philips X'Pert APD diffractometer on five powdered samples, ranging from bedrock to the saprolite zone. The analysis was conducted using a Cu tube with a step size of 0.02°, operating at 40 kV and 40 mA, from 4° to 70° of 2θ CuKa with a 1 s dwelling time. The results revealed the alteration of the minerals occurring in bedrock to those in saprolite, including changes in crystal size. Moreover, the assessment of the mineral phase's crystallinity was conducted by observing the variations in the full width at half maximum (FWHM) of the mineral peak. The crystal size was measured using the Debye-Scherrer equation:

$$D = \frac{k\lambda}{\beta \cos\theta}$$

- k – dimensionless shape factor,
- λ – X-ray wavelength,
- D – crystallite size of the mineral phase acquired through Rietveld refinement,
- θ – peak position in radians,
- β – FWHM.

2.5. SEM-EDS (Scanning electron microscopy with energy dispersive spectrometry)

SEM-EDS method was used for the study of the morphology and structure of five polished thin section samples from bedrock to saprolite, as well as the chemical composition using a Hitachi S-4700 Cold Cathode Field SEM with a NORAN NSS EDS system at the Scanning Electron Microscopy and Microanalysis laboratory, Institute of Geological Sciences, Jagiellonian University. Imaging processes were conducted using secondary electron and back-scattered electron (BSE) modes, while chemical analyses were measured

using a 20 kV accelerating voltage, 10 µA current, and a 100 s counting time. A standardless method was used for the quantification of the element content. Samples were coated with carbon prior to analysis.

3. Result and discussion

3.1. Crystal size and mineral phase

The bedrock is heavily altered by the presence of serpentine, a product of fluid-rock interaction, with approximately 50% of the sample indicating an advanced serpentinization process. The olivine and pyroxene are the dominant minerals in the bedrock, characterized by an interlocking texture, along with serpentine. The olivine abundance in the bedrock, as a primary mineral observed using a polarised microscope, ranges from 50 to 60% and is categorized as peridotite bedrock (Streckeisen 1973). Trace amounts of chromite occur in various shapes and sizes, typically in subhedral form (Figure 3A and 3B). Microscopic observations show that clinopyroxene is more dominant in the saprock than olivine in the bedrock. The olivine appears rough and dissolved under the microscope using plane-polarised transmitted light. Locally, the presence of dissolution cavities is mostly without secondary mineral filling.

The olivine crystals are bluish to greenish without the Fe-oxides effect, while the serpentine veins are colorless and rarely appear with a Fe-oxide stain. The serpentine appears in three types:

- mesh-type,
- Fe-oxides free vein-type, and
- Fe-oxides vein-type.

The vein-type serpentine network contains goethite cross-cutting the primary minerals in the bedrock, resulting in olivine-isolated fragments around 50 to 100 µm in size.

The saprock horizon is partially weathered due to the higher amount of Fe-oxides mineral as a product of the weathering process. The saprock is mainly composed of olivine, clinopyroxene, and serpentine, with a lesser amount of spinel and Fe-bearing minerals. Clinopyroxene occurs as 0.1 to 0.2 mm-sized groups of optically continuous crystals, with individual fragments of around 30 to 100 µm in size. The olivine crystals appear to be dissolved and altered to brownish Fe-oxides at the border (Figure 3C and 3D). Poorly crystalline goethite generally appears as brown-tinged in color in the saprock sample due to the replacement of severely altered olivine. Figure 4 shows the identified minerals in the XRD patterns of the bedrock, saprock, and saprolite horizon samples.

The mineral phases were identified, and the crystal size was determined using the Match by the Crystal Impact and its database. Forsterite and chrysotile dominate the bedrock minerals, with a lower content of enstatite. This reflects the domination of ferromagnesian

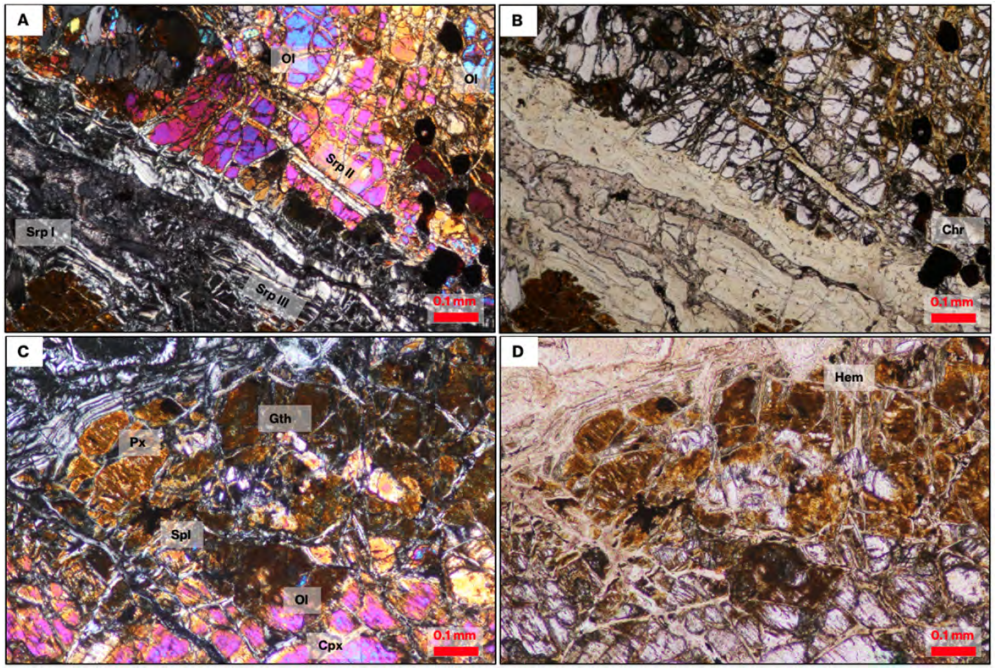

Fig. 3. Photomicrographs of bedrock (A in cross-polarised light and B in plane-polarised light) and saprock (C in XPL and D in PPL) of the study area.
(A, B) olivine distributed widely in the sample cut messy and the vein texture of serpentine.
(C, D) abundancy of clinopyroxene and pyroxene in saprock cut by the serpentine vein with less amount of olivine.
Ol – olivine, Cpx – clinopyroxene, Gth – goethite, Hem – hematite, Px – pyroxene, Srp – serpentine, Chr – chromite, Spl – spinel

Rys. 3. Fotomikrofotografie podłoża skalnego (A w świetle spolaryzowanym krzyżowo i B w świetle spolaryzowanym płasko) i saproku (C w XPL i D w PPL) z badanego obszaru.
(A, B) oliwin szeroko rozprzestrzeniony w próbce, nieuporządkowana tekstura żyły serpentynu.
(C, D) obfitość klinopiroksenu i piroksenu w saproku przeciętym żyłą serpentynu z mniejszą ilością oliwinu

and phyllosilicate minerals in the bedrock. Forsterite was identified in the strong reflection at 5.12 Å and weaker reflections at 3.73 and 3.49 Å, while chrysotile shows a strong reflection at 7.32 Å and weaker reflections at 4.59 and 3.65 Å. Martin and Fyfe (1970), who observed the serpentinization kinetic parameter, introduced a transformation of more than 40 mol% of olivine to chrysotile within a 200 to 325°C temperature range over 200 hours. Those experimental results were assumed by Wegner and Ernst (1983) and Malvoisin et al. (2012) as an indicator of an advanced serpentinization stage where the process is associated with chrysotile production. In the saprock layer, quartz and actinolite are the major minerals, whereas talc and chrysotile occur as accessory constituents. The mineral occurrence in this layer reflects an initial stage of weathering indicated by the presence of talc and goethite.

The major peaks at 4.23 and 3.35 Å are typical of quartz, and those at 3.12 and 8.50 Å correspond to actinolite. The upper, middle, and lower saprolite horizons consist mainly

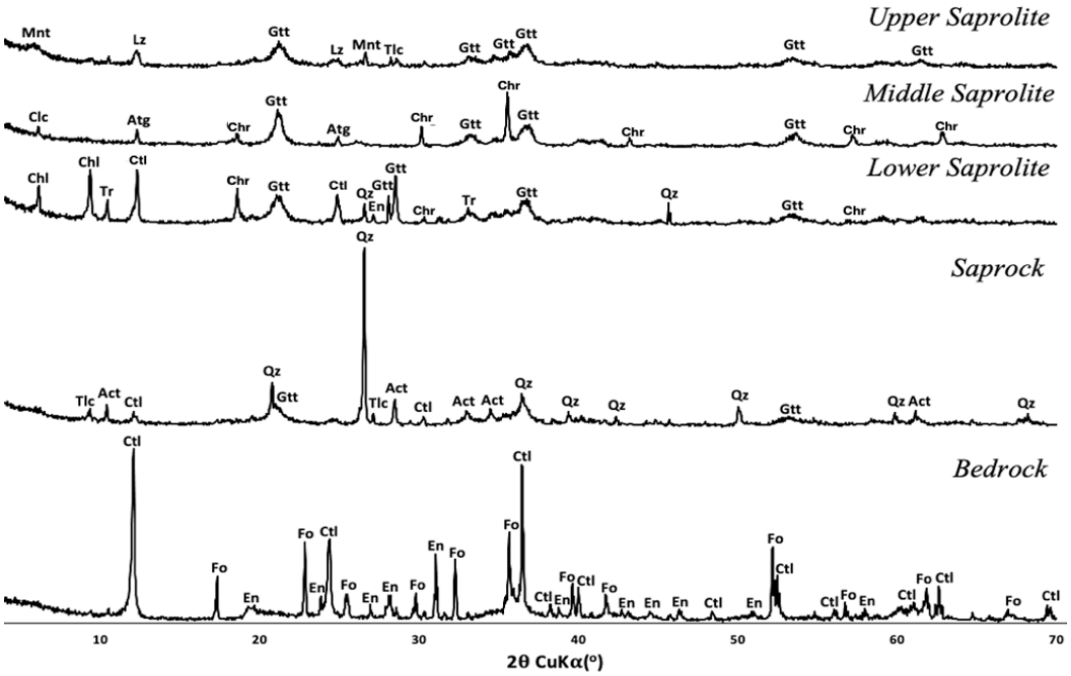

Fig. 4. Stacked diffractograms of bedrock, saprock, lower saprolite, middle saprolite, and upper saprolite from the study area.
Fo – forsterite, En – enstatite, Ctl – chrysotile, Tlc – talc, Act – actinolite, Qz – quartz, Gtt – goethite, Chl – Chlorite, Tr – tremolite, Clc – clinochlore, Atg – antigorite, Chr – chromite, Mnt – montmorillonite, Lz – lizardite

Rys. 4. Ułożone dyfraktogramy podłoża skalnego, saprolitu, dolnego saprolitu, środkowego saprolitu i górnego saprolit z badanego obszaru

of goethite, antigorite, and chlorite, respectively, while montmorillonite, talc, clinochlore, magnetite, and quartz occur in minor amounts. XRD analysis of the saprolite samples shows the strongest reflections of goethite, antigorite, and chlorite at 4.18, 7.18, and 14.41 Å, respectively. The mineral occurrence in the saprolite horizon indicates a significant weathering process characterized by the abundance of Fe-oxide minerals. There is a direct alteration process of serpentine to Fe-oxyhydroxides, such as goethite, without an intermediate phase under the oxidized and acidic setting (Thorne et al. 2009). The mineralogical evidence provided a small amount of serpentine in the form of antigorite in the saprolite horizon, coexisting with goethite, while the hematite is absent. The study proposes that the hematite is the final product of mineral weathering during the sterilization process in the Mandiodo area, where the mineral is probably stable in the limonite horizon to the topsoil layer due to the lower pH and higher content of organic matter. Moreover, Golightly (1981) assumed that in higher Eh and lower pH environments, hematite is more stable compared to goethite.

Further, the goethite will be transformed into hematite under the dehydration process in the lateritic profile. Crystallite size measurements using the Debye-Scherrer equation of the occurred minerals from the saprolite to bedrock layers were calculated using the Rietveld refinement method. The measurement shows the presence of olivine represented by forsterite; enstatite as the only pyroxene group member; chrysotile, antigorite, and lizardite of the serpentine group; actinolite and tremolite from the amphibole group; and clinochlore and chlorite of the chlorite group; while goethite is from Fe-bearing mineral.

Generally, the goethite and chlorite mineral groups experience a size-decreasing trend with depth, while the olivine, pyroxene, amphibole, and serpentine groups reveal an increasing trend of crystal size (Table 1). The initial size of chlorite and goethite is 946.3 and 90.8 Å in the lower saprolite horizon, increasing to 1,797.4 Å in the middle saprolite and 296.6 Å in the upper saprolite. In contrast, the olivine, pyroxene, and serpentine groups occur at 1,841, 1,485.3, and 2,336.9 Å, respectively, but olivine disappears totally in the saprock, and the pyroxene decreases to 214 Å in the lower saprolite. Further, the serpentine shows the most significant crystal size decrease from 2,336.9 Å in the bedrock upwards to 218.4 Å in the upper saprolite horizon. Lastly, the amphibole reduces from 2,202.8 Å in the saprock to 1008.2 Å in the lower saprolite layer. The serpentinisation process involves the hydrothermal alteration of mantle rocks between mid-oceanic ridges and subduction zones in the submarine environments (Lamadrid et al. 2017). Exposed ultramafic rocks subject to the circulation of ~400°C aqueous fluids in the serpentinization process formed serpentine minerals, including lizardite and chrysotile, along with brucite, talc, magnetite, and others (Bach et al. 2004).

Table 1. The crystal size of minerals from bedrock to upper saprolite

Tabela 1. Wielkość kryształów minerałów od podłoża skalnego do górnego saprolitu

Layer	Crystal size (Å)					
	Olivine	Pyroxene	Serpentine	Amphibole	Chlorite	Goethite
Upper saprolite	–	–	218.4	–	–	296.6
Middle saprolite	–	–	991.2	–	1,797.4	155.6
Lower saprolite	–	1,269.3	–	1,008.2	946.3	90.8
Saprock	–	–	2,032.0	2,202.8	–	–
Bedrock	1,841.1	1,485.3	2,336.9	–	–	–

Based on the XRD analysis, the main mineral in the bedrock horizon is composed of forsterite-rich olivine and pyroxene in the form of enstatite (pyroxene rich in enstatite

end-member). Both major minerals are assumed to be the primary minerals altered during hydrothermal alteration, specifically serpentinization, resulting in the formation of serpentine minerals. Constantly, Klein et al. (2015) proposed the chemical equilibrium of the forsterite and enstatite during the serpentinisation process in the bedrock-resulting hydrated product in serpentine.

$$2Mg_2SiO_4 \text{ (Forsterite)} + Mg_2Si_2O_6 \text{ (Enstatite)} + 4H_2O$$

$$= 2Mg_3Si_2O_5(OH)4 \text{ (Serpentine)}$$

Furthermore, the amphibole in the form of actinolite underwent an alteration process, transforming it into serpentine, a finding similar to that of Zhang et al. (2020), who observed corroded actinolite that subsequently altered into serpentine. Above, the reduction in crystallinity of primary minerals (including olivine, pyroxene, and amphibole) to the saprock horizon indicates that the serpentinization stage extends from bedrock to saprock, followed by the initial weathering stage, marked by the presence of chlorite and Fe-bearing minerals, including the growth of their crystal size. Chlorite is the primary clay mineral identified in the study area formed by the chlorite formation process while iron-bearing minerals are mainly in the form of goethite as a result of the oxidation process.

3.2. Mineral chemistry

3.2.1. Olivine

The physical and chemical weathering processes are initiated in tropical climates, coupled with high-intensity rainfall, a lower water table, and continuous tectonic uplift. Those weathering processes dissolve the primary ferromagnesian minerals in the ultramafic rocks.

The dissolution initiated the Fe-oxyhydroxides formation (Roqué-Rosell et al. 2010), followed by the formation of Mg phyllosilicates bearing nickel (Villanova-de-Benavent et al. 2014; Cathelineau et al. 2016; Villanova-de-Benavent et al. 2019). Table 2 reveals the quantification result of the selected olivine, where olivine with higher nickel content is more prevalent than non-nickel olivine. The maximum concentrations of FeO and NiO reach 41.39 and 6.67 wt%, respectively. In general, the nickel content in olivine tends to be lower when compared to serpentine due to their stability. Among the minerals constituting peridotite, such as pyroxene and serpentine (Figure 5), olivine is recognized as the most unstable primary mineral that weathered in the initial stage (Freyssinet et al. 2005).

The calculation of the olivine chemical composition revealed the significant influence of olivine as one of the primary sources of Ni in the study area. Since olivine is recognized

Table 2. The chemical composition of selected olivine, pyroxene, and serpentine (wt%) from the bedrock and saprolite horizons (ND – not determined)

Tabela 2. Skład chemiczny wybranych oliwinów, piroksenów i serpentynów z podłoża skalnego i horyzontów saprolitu

		Bedrock															Saprolite						
Olivine	SiO_2	42.26	44.67	43.06	41.75	42.38	42.49	42.52	41.99	41.56	42.71	42.23	43.14	49.34	42.82	43.72	31.32	42.16	42.32	42.82	46.43	47.3	47.25
	Cr_2O_3	ND	ND	ND	ND	ND	ND	ND	ND	0.4	ND	ND	ND	ND	ND	ND	ND	ND	ND	ND	ND	ND	ND
	MgO	44.17	22.66	45.08	45.32	42.25	45.79	40.93	44.69	45.45	42.95	44.21	45.33	29.71	30.68	30.58	15.99	40.73	42.7	43.35	37.81	36.55	39.62
	FeO	10.45	24.65	10.67	10.58	10.38	9.02	10.49	10.46	10.33	10.82	10.75	9.74	14.32	21.36	19.42	41.39	9.83	10.29	9.38	8.43	8.34	5.69
	CaO	ND	0.85	ND	ND	ND	ND	ND	ND	ND	ND	ND	ND	0.6	0.32	0.6	0.59	ND	ND	ND	0.52	0.27	ND
	MnO	0.11	ND	ND	0.29	ND	ND	ND	ND	ND	ND	ND	ND	ND	ND	ND	1.85	ND	ND	ND	ND	ND	ND
	NiO	1.84	4.42	ND	0.88	3.84	1.7	4.9	1.7	1.9	2.32	1.61	0.7	4.44	2.45	3.52	4.07	5.52	3.54	3.4	5.74	6.61	6.67
	V_2O_5	ND	ND	ND	ND	ND	ND	ND	ND	ND	ND	ND	ND	ND	ND	ND	0.18	0.65	ND	ND	ND	ND	ND
	Total	98.83	97.25	98.81	98.82	98.85	99	98.84	98.84	99.64	98.8	98.8	98.91	98.41	97.63	97.84	95.39	98.89	98.85	98.95	98.93	99.07	99.23
Pyroxene		Bedrock															Saprolite						
	SiO_2	59.11	49.91	58.03	53.68	52.75	60.64	58.74	50.53	54.65	58.5	59.18	57.66	57.79	50.76	54.37	50.82	54.29	58.07	51.79	55.12	51.23	59.1
	Al_2O_3	ND	1.92	1.45	1.45	1.36	ND	1.29	ND	0.96	1.2	ND	1.35	1.2	ND	1.35	2.37	1.87	1.75	ND	0.6	3.55	ND
	Cr_2O_3	0.69	ND	0.67	0.8	1.06	ND	ND	ND	0.44	0.66	0.41	0.92	0.98	ND	1.87	1.17	0.92	0.67	1.43	1.06	1.84	0.55
	MgO	31.79	36.7	31.01	15.5	11.85	29.02	31.65	28.87	21.13	31.03	31.7	30.94	31.15	34.47	30.18	35.04	29.14	31.23	15.63	34.03	14.3	32.27
	FeO	7	10.11	7.5	2.76	2.61	4.73	6.92	17.29	3.61	6.71	7.29	7.47	6.95	11.06	10.52	9.54	6.71	6.74	2.44	4.34	2.56	6.87
	CaO	0.63	0.22	0.52	25.5	26.07	0.27	0.46	0.62	18.41	1.15	0.6	0.5	0.66	1.23	0.53	ND	7.02	0.79	25.74	4.46	26.22	0.44
	NiO	ND	ND	ND	ND	ND	4.36	ND	ND	0.75	ND	ND	0.33	0.5	ND	ND	ND	ND	ND	ND	ND	ND	ND
	Total	99.22	98.86	99.18	99.69	95.7	99.02	99.06	97.31	99.95	99.25	99.18	99.17	99.23	97.52	98.82	98.94	99.95	99.25	97.03	99.61	99.7	99.23
Serpentine		Bedrock												Saprolite									
	SiO_2	46.48	45.89	49.74	50.35	45.57	45.22	48.74	49.14	48.75	44.36	46.82	51.3	48.89	47.97	49.58	46.25	48.58	49.04	45.68	47.75	47.19	50.07
	Al_2O_3	ND	2.21	ND	ND	3.14	ND	ND	ND	ND	ND	ND	ND	ND	ND	ND	ND	ND	ND	ND	ND	ND	ND
	Cr_2O_3	ND	1.42	ND	ND	2.04	ND	0.46	ND	ND	ND	ND	ND	ND	ND	ND	ND	ND	ND	ND	ND	1.13	0.38
	MgO	40.52	40.06	39.02	38.46	38.72	39.14	41.54	39.45	37.91	43.66	40.89	38.88	38.91	37.84	38.14	28.55	37.01	37.49	34.86	36.97	33.56	35.58
	FeO	12.17	8.2	9.54	9.08	9.04	10.8	6.73	8.25	10.28	9.34	10.68	6.19	6.23	9.05	7.13	10.84	8.59	7.17	11.03	9.39	10.94	7.79
	CaO	ND	1.3	ND	ND	ND	ND	ND	ND	ND	ND	ND	0.19	0.87	ND	ND	0.61	ND	ND	0.48	ND	0.27	0.35
	MnO	ND	ND	ND	ND	ND	ND	ND	ND	ND	ND	ND	ND	ND	ND	ND	5.28	ND	0.25	0.76	ND	ND	ND
	NiO	0.52	0.91	1.63	1.28	1.48	4.75	2.2	2.9	3.04	2.59	1.57	3.34	5.09	5.13	5.07	7.25	5.78	5.98	7.14	5.88	6.76	5.81
	Total	99.69	100	99.94	99.18	99.99	99.92	99.67	99.74	99.98	99.96	99.96	99.91	99.99	99.99	99.92	98.78	99.96	99.93	99.95	99.99	99.85	99.98

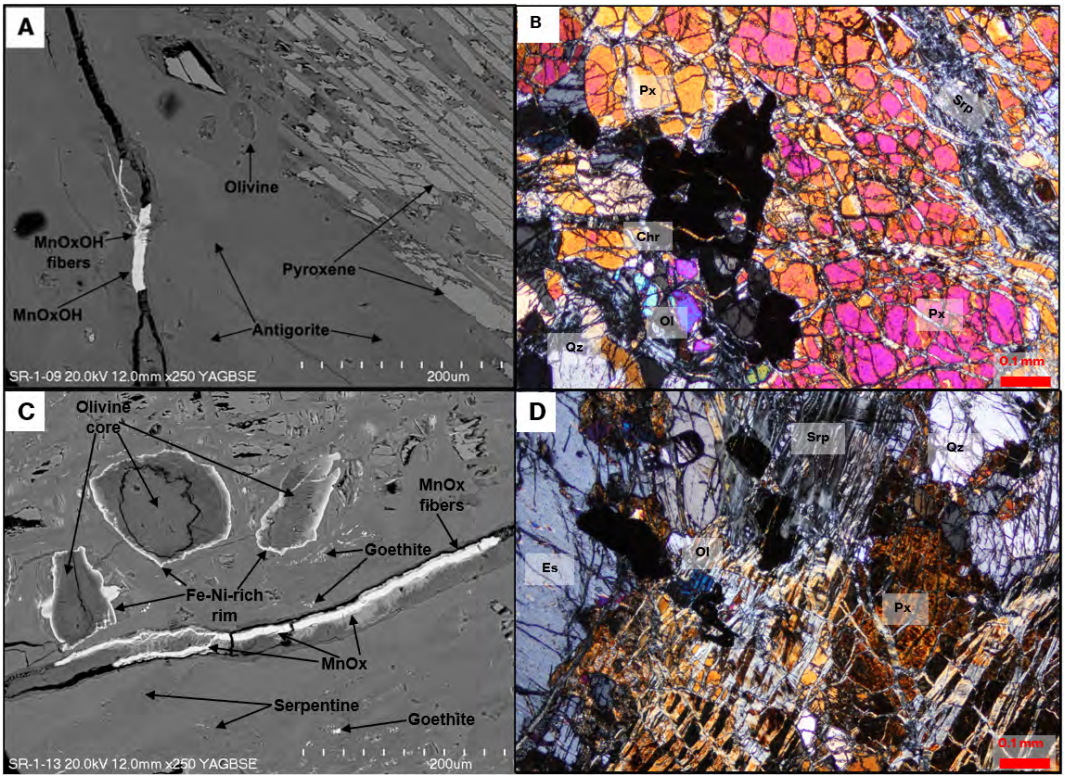

Fig. 5. BSE image of olivine with zoning texture, showing (A,C) lower Ni content in the core compared to the rim, (B) interlocking texture of olivine, pyroxene, and serpentine in the bedrock with minor amount of quartz (D) in cross-polarised light.
Ol – olivine, Es – enstatite, Qz – quartz, Px – pyroxene, Srp – serpentine, Chr – chromite

Rys. 5. Obraz BSE oliwinu, piroksenu i serpentynu

as the primary nickel-bearing mineral in the protolith, nickel is released due to weathering but is subsequently retained within the profile through absorption by goethite. Freyssinet et al. (2005) and Domínguez-Carretero et al. (2024) described that as the weathering process persists, goethite may experience a dissolution and reprecipitation process followed by Ni leaching. Furthermore, goethite released Ni, which was then trapped in the hydrothermal serpentine from the protolith that formed before the lateralization and weathering of the peridotite bedrock, contributing to the secondary Fe-Ni-rich serpentine formation.

3.2.2. Pyroxene

The initial serpentinization process of olivine and pyroxene, followed by ophiolite weathering, resulted in the formation of Fe-oxyhydroxides, silica, gypsum, pyrite, and quartz

(Schwertmann and Taylor 1989). Together with the leaching of Mg and Si, the weathering of Ni-rich olivine and pyroxene resulted in the formation of goethite or hematite and smectite, influenced by the intense humid tropical conditions (Domènech et al. 2017). The occurrence of pyroxene in the bedrock and saprock samples is relatively high. The optical microscope image (Figure 5) illustrates the pyroxene structures, revealing predominantly granular formations associated with olivine and serpentine. Klein et al. (2015) explained the interaction of meteoric water with olivine and pyroxene, the primary minerals in ultramafic rocks, as they transform into serpentine, a hydrous magnesium silicate, through the weathering process. Random pyroxene samples were selected for the quantification of elemental content analysis using EDS, as presented in Table 2. FeO reaches 17.29 wt%, whereas Ni is 4.36 wt% in the measured pyroxene, indicating that most of the pyroxene is categorized as nickel-devoid due to the lower content of Ni. Chemical weathering of ultramafic bedrock containing Ni-Co-rich olivine and pyroxene led to the formation of smectite, serpentine, and silicate containing Fe, Mg, Ni, and Co. At the same time, the Al resulted from the volcanic rocks (Helvaci et al. 2018). Compared to olivine and serpentine as the dominant minerals, pyroxene is the primary source of Al in the bedrock.

3.2.3. Serpentine

Serpentinization occurs when aqueous fluids interact hydrothermally, typically at temperatures below approximately 450°C, with the Mg-Fe-rich minerals found in the lithospheric mantle, such as olivine and pyroxenes (Mével, 2003; Evans et al. 2013). Tauler et al. (2007) categorized serpentine into two types:

- primary (hydrothermal) serpentine (referred to as serpentine I), which forms a mesh texture around olivine grains and has low Ni and Fe content similar to primary olivine, and
- serpentine II, also known as “primary weathered serpentine” (Pelletier 1996) or “altered primary serpentine” (Freyssinet et al. 2005), where the serpentine II has lower Mg content and higher concentrations of Fe and Ni compared to serpentine I.

In the study area, randomly chosen serpentine samples were analyzed using EDS, and the resulting element contents are presented in Table 2. Nickel-rich serpentine surpasses the non-nickel serpentine in EDS measurement. The highest recorded NiO concentration reaches 7.25 wt%, while the FeO content ranges from 6.19 to 12.17 wt%.

In comparison to olivine and pyroxene, serpentine exhibits significantly higher Ni content. The results indicate that serpentine, together with olivine, is the primary source of nickel in the study area. Notably, an increase in Ni concentration in serpentine corresponds to a decrease in Mg concentration, as Ni or Fe replaces Mg atoms. The substitution of Mg^{2+} by Ni^{2+} and/or Fe^{3+} in serpentine stabilizes the silica excess resulting from the serpentine incongruent dissolution, initiating the leaching of Mg^{2+}. Freyssinet et al. (2005) proposed that Ni replaces Mg in serpentine II octahedral sites without involving solution, recrystallization, or neoformation processes.

3.2.4. Pentlandite

Pentlandite is one of the sulfide minerals mostly found in mafic or ultramafic rocks associated with pyrrhotite and chalcopyrite in hydrothermal settings (Staude et al. 2023). The formation of pentlandite in the Fe-Cu-Ni-S system was described by Barnes et al. (2020) as resulting from the exsolution of Fe-Ni monosulphide at high temperature or from the peritectic reaction of residual melt and monosulphide solid solution (MSS) along the solidification of Fe-Ni-Cu sulfide liquids.

Studies of pentlandite in nickel deposits using microbeam techniques have shown that the occurrence of Re, Os, Ir, Ru, Rh, Pd, and Co is hosted mainly by pentlandite (Dare et al. 2010; Pagé et al. 2012). The presence of pentlandite in octahedral cleavage with a magnetite rim in the bedrock sample indicates a weathering process in the bedrock. Further, Barnes et al. (2020) assumed that there is a significant correlation between the association of pentlandite and chalcopyrite in the elevation of PGE, specifically the Pd concentration. Most of the pentlandite appears associated with chalcopyrite and pyrite along the serpentine vein in octahedral cleavage (Figure 6).

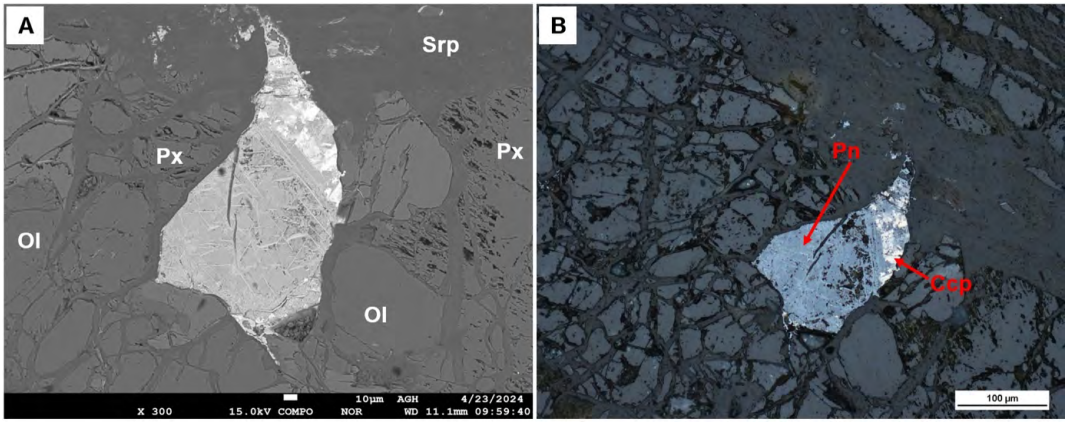

Fig. 6. BSE images (A) and photomicrographs of pentlandite in reflected light (B) from the bedrock horizon. (A) pentlandite with octahedral cleavage with the intergrowth of chalcopyrite surrounded by olivine, pyroxene, and serpentine.
Ol – olivine, Srp – serpentine, Px – pyroxene, Ccp – chalcopyrite, Pn – pentlandite

Rys. 6. Obrazy BSE i mikrofotografie pentlandytu

The implication of the pentlandite presence in the lateritic nickel deposit led to the indication of PGE occurrence in the sulfide minerals. Thirteen randomly selected pentlandite samples from the study area were quantified by EDS, as presented in Table 3. Table 3 shows an abundance of Ni and Fe in pentlandite, compared to olivine and serpentine, in the bedrock and saprolite horizons. The average concentration of Ni in the bedrock and saprock

Table 3. The chemical composition of selected pentlandite, Mn-oxides, chromite, and goethite (wt%) from the bedrock and saprolite horizons (ND – not determined)

Tabela 3. Skład chemiczny wybranych pentlandytów, tlenków manganu, chromitu i getytu z podłoża skalnego i horyzontów saprolitu

Pentlandite		Bedrock							Average	Saprock						Average	
	Fe	33.73	37.27	34.6	34.02	29.96	43.11	37.23	35.7	35.28	34.53	33.84	32.73	34.82	44.91	36.01	
	Ni	30.81	26.82	30.09	29.91	32.14	20.55	28.48	28.4	29.98	30.05	27.59	31.58	27.92	18.36	27.58	
	S	33.96	34.25	33.83	33.74	34.22	34.64	32.4	33.86	32.98	33.97	36.21	34.2	35.41	34.91	34.61	
	Mg	0.74	0.89	0.87	1.21	1.75	1.02	1.02	1.07	0.79	0.77	0.78	0.74	0.82	0.88	0.79	
	Si	0.76	0.76	0.61	0.66	1.93	0.68	0.87	0.89	0.95	0.67	1.2	0.75	0.91	0.83	0.88	
Mn-Oxides		Bedrock								Saprolite							
	MnO	58.87	59.26	60.03	59.97	58.91	60.14	56.93	59.74	57.27	58.76	59.73	59.98	57.92	59.87		
	NiO	29.77	26.63	26.12	30.14	28.87	25.93	29.47	29.98	28.17	27.27	27.16	30.23	29.64	31.48		
	CoO	2.51	5.48	4.85	2.17	3.02	5.04	6.03	3.15	7.48	6.64	5.54	2.76	4.84	2.25		
	Fe_2O_3	ND	0.15	0.19	ND	0.08	0.11	ND	ND	ND	ND	ND	ND	0.06	ND		
	MgO	4.49	4.17	4.09	3.96	4.52	4	3.83	3.79	3.8	3.67	3.28	3.41	3.82	3.37		
	SiO_2	4.12	3.61	3.9	3.69	4.02	3.86	3.37	3.1	2.72	2.94	3.34	3.28	3.37	2.91		
	CaO	0.24	0.69	0.81	0.07	0.56	0.92	0.37	0.24	0.56	0.71	0.95	0.34	0.35	0.11		
	Total	100	99.99	99.99	100	99.98	100	100	100	100	99.99	100	100	100	99.99		
Chromite		Bedrock										Saprolite					
	Cr_2O_3	30.52	31.45	30.59	24	30.98	29.42	30.18	31.7	21.03	30.44	38	45.96	40.03	40.03	39.56	34.98
	Al_2O_3	32.65	34.25	35.44	42.07	35.37	37.43	35.4	33.93	46.13	36.16	26.7	18.13	23.96	23.96	27.01	31.39
	Fe_2O_3	21.88	19.27	18.76	18.15	19.09	16.95	19.58	19.78	15.84	18.36	23.35	26.24	24.75	24.75	20.87	19.54
	MgO	12.47	13.94	13.92	14.81	13.13	14.92	13.36	13.21	16.39	14.17	10.8	7.02	10.42	10.42	11.7	13.32
	SiO_2	2.18	0.86	1.06	0.96	1	1.28	1.32	1.04	0.6	0.87	1.15	1.87	0.84	0.84	0.86	0.77
	V_2O_5	0.3	ND	ND	ND	0.43	ND	0.15	0.34	ND	ND	ND	0.78	ND	ND	ND	ND
	MnO	ND	0.23	0.22	ND	ND	ND	ND	ND	ND	ND	ND	ND	ND	ND	ND	ND
	Total	100	100	99.99	99.99	100	100	99.99	100	99.99	100	100	100	100	100	100	100
Goethite		Bedrock				Saprolite											
	Fe_2O_3	88.41	94.84	88.84	92.12	94.82	93.27	90.08	98.26	97.93	94.53	93.87					
	NiO	0.42	0.03	3.49	0.17	ND	0.25	3.33	ND	ND	1.96	1.56					
	MnO	1.89	0.83	ND	0.32	0.81	1	1.81	0.46	0.91	ND	0.96					
	MgO	4.48	1.12	4.33	3.17	1.8	1.72	2.13	0.53	0.3	1.36	1.22					
	SiO_2	4.8	3.17	3.34	4.22	2.57	3.75	2.65	0.75	0.86	2.14	2.39					
	Total	100	99.99	100	100	100	99.99	100	100	100	99.99	100					

horizons depletes from 28.40 to 27.58 wt%, while the Fe shows an opposite trend. The Fe content increases from 35.70 to 36.01 wt% from the bedrock to the saprock, which was likely influenced by the weathering process. In comparison, the Ni and Fe concentrations in pentlandite are relatively higher compared to olivine and serpentine but are very low in the comparison of abundance.

3.2.5. Mn-oxides

The dissolution of primary silicates initiates the formation of poorly crystallized goethite, releasing Mn and Co in the saprolite horizon. This process occurs through the adsorption and replacement of iron in the oxide structure (Gerth 1990; Singh et al. 2002). Table 3 illustrates the quantification result of the selected Mn-oxides from the bedrock and saprock horizon samples. The maximum concentrations of MnO and NiO reached 60.14 and 30.23 wt%, respectively, while the CoO content was up to 7.48 wt%. The Mn-oxides show a similar trend with pentlandite, where the Ni content in those minerals is relatively higher compared to olivine and serpentine but much lower in terms of abundance.

The study conducted by Marker et al. (1991) and Ulrich et al. (2019) suggested that the Mn and Co leaching process in the upper part of the weathering profile led to the formation of Mn oxides. The Mn-oxides in the bedrock and saprock (Figure 7) can be divided into two types:

- Mn-oxides that filled the crack in the serpentine veins, characterized with a very high concentration of MnO; compared to
- Mn-Fe-Ni mixture that appears in messy texture contained a balanced concentration of Mn and Fe with lower Ni.

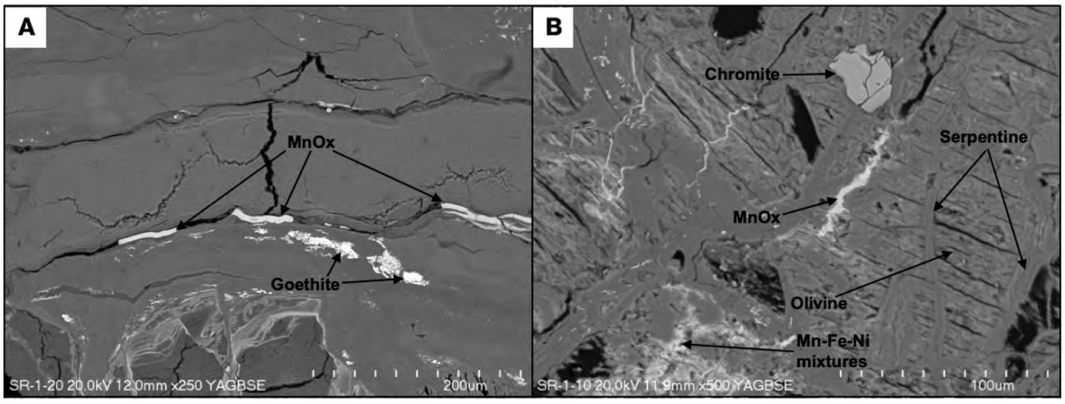

Fig. 7. (A) BSE image of Mn-oxides filled the serpentine crack, and (B) some mixtures of Mn-Fe-Ni and chromite in the saprock

Rys. 7. Obraz BSE tlenków Mn

3.2.6. Chromite

Chromite is the main chromium-bearing mineral in the ultramafic rocks that occur in the study area. Fendorf (1995) proposed a result from thermodynamic and field studies where the chromite is unstable in lateritic deposits, implying that Cr in laterite is a weathering product of ultramafic rocks and is depleted in the uppermost part of the profile. Further, the author suggested that chromite is the primary host of Al in the wehrlite due to its stability. In supergene environments, chromium in the form of chromite is immobile (Becquer et al. 2003). In the study area, chromite is divided into:

- primary chromite characterized by the higher content of Al, and
- weathered or secondary chromite identified by the higher content of Cr in the core with high Fe in their rim or border part.

Sixteen random chromites from the samples were selected for elemental content analysis using EDS, with the results presented in Table 3. The maximum concentrations of Cr_2O_3 and Al_2O_3 reach 45.96 and 46.13 wt%, respectively. On average, the concentrations of Cr_2O_3 and Al_2O_3 are 33.05% and 32.5%, respectively. In general, Cr_2O_3 and Al_2O_3 distribution reveals a strong alumina–chromium association due to their concentration in chromite. Primary chromites are the primary host of Cr and V due to their resistance to weathering compared to other minerals. Conversely, Fe from pyroxene dissolution enters into the goethite structure without the Cr and V fraction (Figure 8).

Consequently, both elements experience continuous enrichment with increasing levels of weathering (Ulrich et al. 2019; Santoro et al. 2022). Eliopoulos et al. (2012) and Helvaci et al. (2018) highlighted that chromite and Mn, Co, and Ni oxide phases are the primary hosts of Mn, Co, and Ni in the saprolite horizon at Bitincka (Albania) and Gördes (Turkey).

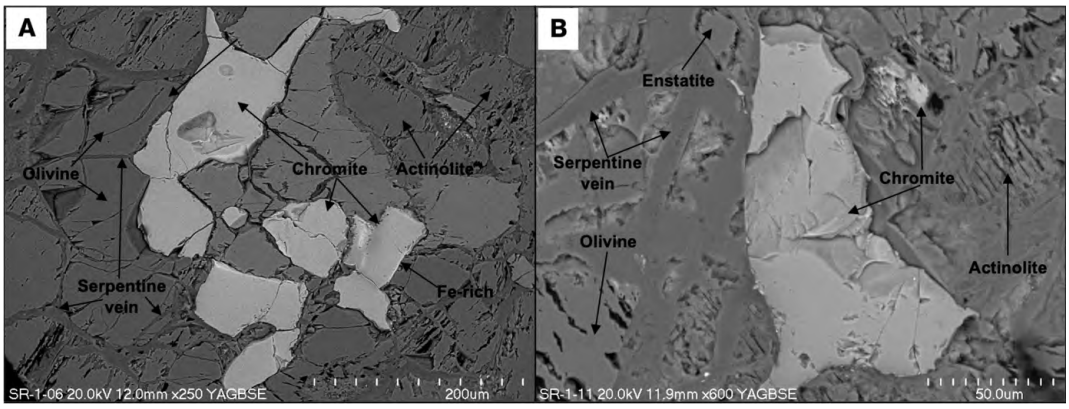

Fig. 8. (A,B) BSE image of the interlocking texture of chromite, olivine, and serpentine with a higher concentration of Fe in the border part

Rys. 8. Obraz BSE splecionej tekstury chromitu, oliwinu i serpentynu

3.2.7. Goethite

Supergene weathering during the evolution of the laterite profile resulted in dynamic processes that altered the physicochemical properties of goethite (Golightly, 1981; Freyssinet et al. 2005; Butt and Cluzel 2013; Fu et al. 2014). In lateritic deposits, pyroxene, olivine, and serpentine were replaced by goethite and serpentine II (Tauler et al. 2017). Goethite crystallization occurs through the aging of an amorphous (or poorly crystalline) ferric oxide precursor, ferrihydrite, with a preference for goethite formation at either acidic pH (< 4) or highly alkaline pH (> 12) (Dublet et al. 2015; Myagkiy et al. 2017; Wells et al. 2022). Hematite formation, on the other hand, is promoted at a nearly neutral pH (7–8) (Schwertmann and Murad 1983; Cornell et al. 1987; Wells et al. 2022). Eleven randomly selected goethites from the study area were quantified by EDS, as presented in Table 3. The concentration of Fe_2O_3 in goethite ranges from 88.41 to 98.26 wt%, with a minor amount of NiO and MnO. The majority of the goethite and Fe-bearing minerals in the bedrock zone occur along the serpentine veinlet or in the border part of pyroxene, olivine, and serpentine as a result of the weathering process of those minerals. Furthermore, saprock is primarily found in association with Mn-Fe-Ni mixtures that appear in a messy texture (Figure 7). The presence of the goethite and Fe-bearing minerals in the bedrock indicates an oxidation process of olivine, pyroxene, and serpentine in the bedrock. This process marks the beginning of the weathering stage following advanced serpentinization in the bedrock.

3.3. Major element distribution

The peridotite bedrock is composed mainly of significant elements of Mg and Si, as reflected in the XRD result, which also indicates the abundance of olivine and serpentine, both of which are composed of these elements. Elements such as Fe, Ni, Cr, Mn, and Al occur in low concentrations. Ferromagnesian minerals from the weathering process in the bedrock (Figure 9) led to the formation of Fe-oxides, which retained partially minor and trace elements such as Ni, Co, Cu, and Mn, followed by a significant loss of Mg and Si (Anand and Payne, 2002). The silica reduction during the lateritisation process, under limited drainage conditions, followed by the leaching process, led to the development of a cemented secondary silica zone in the upper layer of the laterite deposit (Herdianita et al. 2000; Ece et al. 2013). The major geochemistry of the saprolite zone provides a significant elevation of Fe up to 43.8 wt% in the upper saprolite layer compared to the saprock and bedrock horizon. In contrast, Si and Mg decrease drastically from 22.14% and 23.22% in the bedrock to 7.3% and 3.9% in the upper saprolite, respectively. The significant change in the concentration of the element from the peridotite bedrock to saprolite resulting from the serpentinization and weathering process leads to the dissolution of ferromagnesian minerals.

Mg and Si are more soluble, causing their depletion closer to the surface, while the other elements, including Fe, Ni, Cr, Mn, and Al, are retained in the weathered horizon (Eliopoulos

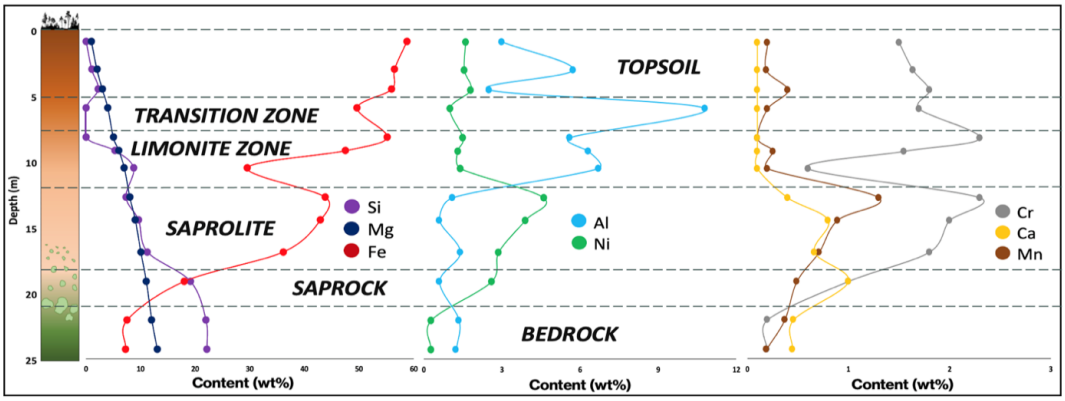

Fig. 9. Major element distribution from bedrock to topsoil in the Ni-laterite profile in the Mandiodo area

Rys. 9. Dystrybucja głównych pierwiastków od podłoża skalnego do gleby wierzchniej w profilu Ni-laterytu w obszarze Mandiodo

et al. 2012). Geologically, the plate movement caused a regional uplift of Sulawesi Island from the Eocene to the present (Golightly and Arancibia 1979; Kadarusman et al. 2004), thus elevating the terrain, lowering the groundwater level, and deepening the weathering front (Butt and Cluzel 2013). Due to the deepening, the impact of oxidation during lateralization appears to be relatively weak; however, groundwater fluctuation and rock–water interaction tend to be more significant and related to the weathering process. The fluctuation enhances bedrock decomposition and initiates mineral alteration. Ni-rich olivine, as a primary mineral in peridotite, experienced a leaching process that produced Fe-oxides, causing the abundance of Fe in the saprolite horizon. Furthermore, the favorable ion exchange between serpentine and leaching solution released Ni adsorbed by goethite or substituted the Mg in serpentine (Golightly and Arancibia 1979).

Chromite, as an accessory mineral, plays a significant role in the occurrence of Cr and Al in both bedrock and serpentine horizons. The geochemical variation of the profile shows a potential of Cr and Al in the lateritic nickel deposit. Cr is drastically enriched together with Ni in the saprolite horizon, while Al slightly increases in the limonite zone and is significantly deposited in the transition zone. The content of Al and Cr in chromite, according to Pagé and Barnes (2009), is not influenced by the subsolidus process or re-equilibration with olivine, which reflects the original melt composition, tectonic setting, and the crystallization environment. Moreover, the very Al content in the bedrock and saprolite horizons, which drastically increases in the limonite and transition zone, shows a significant influence of pH in Al-bearing minerals' formation, where the pH value in the bedrock and saprolite horizons is not low enough for the crystallization of Al-bearing minerals. Schellmann (1994) suggested that lowering pH values influenced by rainwater percolation caused a very effective weathering of ultramafic rocks due to the aluminum solubility. According to the

EDS quantification results of olivine, pyroxene, and serpentine, the main minerals in the bedrock, pyroxene appears to be the primary host of Al in the bedrock. At the same time, the Al-rich chromite is the primary host in the saprolite horizon. Lastly, the formation of Mn-oxides in the lateritic profile is influenced by the transition of the soil solution from an acidic to a slightly alkaline state (Ulrich et al. 2019). Manganese is commonly immobilized by Fe-bearing minerals in the oxide-rich zone. Quantin et al. (2002) explained that weathering, temperature, and humidity influence the leaching of Mn from Fe-bearing minerals, causing downward transportation in the form of colloidal or aqueous complexes.

Ni and Cr enriched significantly towards the saprolite horizon from 0.26 to 4.6 wt% and from 0.19 to 2.3 wt%, respectively, while Al, Ca, and Mn increased moderately. The Ni abundance in saprock and saprolite horizons is primarily hosted by olivine and serpentine. Cr and Al are hosted by chromite, while Mn-oxides host the Mn. The geochemical variation of Ni in the Mandiodo area shows a similar trend with the lateritic nickel deposit in Halmahera Island (Konopka et al. 2022), where the Ni experienced a significant enrichment from saprock to saprolite horizon up to before the drastic depletion in the limonite zone to topsoil layer. The variation suggests the importance of the saprolite horizon as a nickel ore zone, followed by the saprock layer, which is primarily hosted by serpentine. Currently, nickel extraction requires a fluctuating cut-off grade (COG) based on the nickel demand price, where the COG is elevated if the demand price decreases, and vice versa. Generally, the rotary kiln electric furnace (RKEF) method, applied to high-grade nickel ore, required 1.75 wt% Ni, while the high-pressure acid leach (HPAL) method, applied to low-grade nickel ore with high Fe content, required 1 wt% Ni. According to Dalvi et al. (2004) and Konopka et al. (2022), a lateritic nickel deposit containing Ni > 0.9 wt% is suitable for consideration as economic. The higher content of Ni in the saprock layer (up to 2.9 wt%) – comprising mostly soft material – offered an economic prospect for future extraction, as the Ni concentration exceeded the minimum requirements. Implementing the blending method for the saprock materials with the saprolite ore containing a higher concentration of Ni would be a beneficial method to increase the Ni content of the materials to elevate the economic value of the saprock layer.

Conclusions

1. The bedrock in the study area is categorized as peridotite, primarily composed of olivine, pyroxene, and serpentine.
2. The mineralogical characteristic of the bedrock reflects an advanced serpentinization process, while the saprock and saprolite indicate an initial stage of weathering.
3. Ni in the saprolite horizon is primarily hosted through serpentine group minerals, with a minor occurrence in goethite.
4. The nickel content in sulfide minerals is relatively higher compared to serpentine and olivine minerals but lower in mineral abundance.

5. The geochemical study revealed a positive correlation between Ni and Fe, which was negatively correlated with Si and Mg, while other transition metals increased slightly towards the saprolite horizon.
6. The geochemical variations of Cr in the saprolite horizon and Al in the limonite and transition zones indicate the potential for future critical metal resources.

This work has been funded and logistically supported by the "Research Support Module" and the publication has been supported by a grant from the Faculty of Geography and Geology under the Strategic Programme Excellence Initiative at Jagiellonian University. The authors kindly thank Mr. Djamaluddin for his assistance during the sample collection. The authors acknowledge the support from PT. ANTAM – UBPN Konawe Utara for approval of the sample collection. Finally, we thank the anonymous reviewers for their time, comments, and suggestions which much improved the paper.

The Authors have no conflict of interest to declare.

REFERENCES

Anand, R.R. and Paine, M., 2002. Regolith geology of the Yilgarn Craton, Western Australia: Implications for exploration. *Australian Journal of Earth Sciences* 49, pp. 3–162, DOI: 10.1046/J.1440-0952.2002.00912.X.

Bach et al. 2004 – Bach, W., Garrido, C.J., Paulick, H., Harvey, J. and Rosner, M. 2004. Seawater-peridotite interactions: First insights from ODP Leg 209, MAR 15°N. *Geochemistry, Geophysics, Geosystems* 5, pp. 9–26, DOI: 10.1029/2004GC000744.

Barnes et al. 2020 – Barnes, S.J., Taranovic, V., Schoneveld, L.E., Mansur, E.T., le Vaillant, M., Dare, S., Staude, S., Evans, N.J. and Blanks, D. 2020. The occurrence and origin of pentlandite-chalcopyrite-pyrrhotite loop textures in magmatic Ni-Cu sulfide ores. *Economic Geology* 115, pp. 1777–1798, DOI: 10.5382/ECONGEO.4757.

Becquer et al. 2003 – Becquer, T., Quantin, C., Sicot, M. and Boudot, J.P., 2003. Chromium availability in ultramafic soils from New Caledonia. Science of The Total Environment, 301: 251–261, DOI: 10.1016/S0048-9697(02)00298-X.

Brand et al. 1998 – Brand, N.W., Butt, C.R.M. and Elias, M. 1998. Nickel Laterites: Classifications and Features. *AGSO Journal of Australian Geology & Geophysics* 17, pp. 81–88.

Butt, C.R.M. and Cluzel, D. 2013. Nickel Laterite Ore Deposits: Weathered Serpentinites. *Elements* 9, pp. 123–128, DOI: 10.2113/GSELEMENTS.9.2.123.

Cathelineau et al. 2016 – Cathelineau, M., Quesnel, B., Gautier, P., Boulvais, P., Couteau, C. and Drouillet, M., 2016. Nickel dispersion and enrichment at the bottom of the regolith: formation of pimelite target-like ores in rock block joints (Koniambo Ni deposit, New Caledonia). *Mineralium Deposita* 51(2), pp. 271–282, DOI: 10.1007/s00126-015-0607-y.

Cornell et al. 1987 – Cornell, R.M., Giovanoli, R. and Schindler, P.W. 1987. Effect of Silicate Species on the Transformation of Ferrihydrite into Goethite and Hematite in Alkaline Media. *Clays and Clay Minerals* 35, pp. 21–28, DOI: 10.1346/CCMN.1987.0350103.

Dalvi et al. 2004 – Dalvi, A.D., Bacon, W.G. and Osborne, R.C. 2004. The Past and the Future of Nickel Laterites. In Proceedings of the PDAC 2004 International Convention, Trade Show & Investors Exchange, Mississauga, ON, Canada, 7–10 March 2004.

Dare et al. 2010 – Dare, S.A.S., Barnes, S.J. and Prichard, H.M. 2010. The distribution of platinum group elements (PGE) and other chalcophile elements among sulfides from the Creighton Ni-Cu-PGE sulfide deposit, Sudbury, Canada, and the origin of palladium in pentlandite. *Mineralium Deposita* 45, pp. 765–793, DOI: 10.1007/s00126-010-0295-6.

Domènech et al. 2017 – Domènech, C., Galí, S., Villanova-de-Benavent, C., Soler, J.M. and Proenza, J.A. 2017. Reactive transport model of the formation of oxide-type Ni-laterite profiles (Punta Gorda, Moa Bay, Cuba). *Mineralium Deposita* 52, pp. 993–1010, DOI: 10.1007/s00126-017-0713-0.

Domínguez-Carretero et al. 2024 – Domínguez-Carretero, D., Proenza, J. A., Villanova-de-Benavent, C., Aiglsperger, T., Tauler, E., Rojas-Purón, A., Duque, N., González-Jiménez, J.-M., Garcia-Casco, A. and Galí, S. 2024. The Geology, Geochemistry, and Mineralogy of the Moa Bay Ni Laterite Mining District, Cuba. *Economic Geology* 119, pp. 1685–1706, DOI: 10.5382/ECONGEO.5101.

Dublet et al. 2015 – Dublet, G., Juillot, F., Morin, G., Fritsch, E., Fandeur, D. and Brown, G.E. 2015. Goethite aging explains Ni depletion in upper units of ultramafic lateritic ores from New Caledonia. *Geochimica et Cosmochimica Acta* 160, pp. 1–15, DOI: 10.1016/J.GCA.2015.03.015.

Ece et al. 2013 – Ece, Ö.I., Ekinci, B., Schroeder, P.A., Crowe, D. and Esenli, F. 2013. Origin of the Düvertepe kaolin–alunite deposits in Simav Graben, Turkey: Timing and styles of hydrothermal mineralization. *Journal of Volcanology and Geothermal Research* 255, pp. 57–78, DOI: 10.1016/J.JVOLGEORES.2013.01.012.

Elias, M. 2002. *Nickel Lateritic Deposits-Geological Overview, Resources and Exploitation*. [In:] *Giant Ore Deposits: Characteristics, genesis and exploration*, eds DR Cooke, D.R. and Pongratz, J. *CODES Special Publication* 4, Centre for Ore Deposit Research, University of Tasmania, pp. 205–220.

Eliopoulos et al. 2012 – Eliopoulos, D.G., Economou-Eliopoulos, M., Apostolikas, A. and Golightly, J.P. 2012. Geochemical features of nickel-laterite deposits from the Balkan Peninsula and Gordes, Turkey: The genetic and environmental significance of arsenic. *Ore Geology Reviews* 48, pp. 413–427, DOI: 10.1016/J.OREGEOREV.2012.05.008.

Evans et al. 2013 – Evans, B.W., Hattori, K. and Baronnet, A. 2013. Serpentinite: What, Why, Where? *Elements* 9(2), pp. 99–106, DOI: 10.2113/GSELEMENTS.9.2.99.

Fendorf, S.E. 1995. Surface reactions of chromium in soils and waters. *Geoderma* 67, pp. 55–71, DOI: 10.1016/0016-7061(94)00062-F.

Freyssinet et al. 2005 – Freyssinet, P.H., Butt, C.R.M., Morris, R.C. and Piantone, P. 2005. *Ore-Forming Processes Related to Lateritic Weathering*. [In:] Hedenquist, J.W., Thompson, J.F.H., Goldfarb, R.J. and Richards, J.W. *One Hundredth Anniversary Volume. Society of Economic Geologist*, Canada, pp. 681–722, DOI: 10.5382/AV100.21.

Fu et al. 2014 – Fu, W., Yang, J., Yang, M., Pang, B., Liu, X., Niu, H. and Huang, X. 2014. Mineralogical and geochemical characteristics of a serpentinite-derived laterite profile from East Sulawesi, Indonesia: Implications for the lateritization process and Ni supergene enrichment in the tropical rainforest. *Journal of Asian Earth Sciences* 93, pp. 74–88, DOI: 10.1016/J.JSEAES.2014.06.030.

Gerth, J. 1990. Unit-cell dimensions of pure and trace metal-associated goethites. *Geochimica et Cosmochimica Acta* 54, pp. 363–371, DOI: 10.1016/0016-7037(90)90325-F.

Golightly, J.P., 1981. *Nickeliferous Laterite Deposits. Economic Geology, Seventy-Fifth Anniversary Volume (1905––1980)*, pp. 710–734, DOI: 10.5382/AV75.18.

Golightly, J.P. and Arancibia, O.N. 1979. The chemical composition and infrared spectrum of nickel- and iron-substituted serpentine form a nickeliferous laterite profile, Soroako, Indonesia. *Can Mineral* 17, pp. 719–728.

Hall, R. and Wilson, M.E.J. 2000. Neogene sutures in eastern Indonesia. *Journal of Asian Earth Sciences* 18, pp. 781–808, DOI: 10.1016/S1367-9120(00)00040-7.

Helvaci et al. 2018 – Helvaci, C., Oyman, T., Gündoğan, İ., Sözbilir, H., Parlak, O., Kadir, S. and Güven, N. 2018. Mineralogy and genesis of the Ni–Co lateritic regolith deposit of the Çaldağ area (Manisa, western Anatolia), Turkey. *Canadian Journal of Earth Sciences* 55, pp. 252–271, DOI: 10.1139/cjes-2017-0184.

Herdianita et al. 2000 – Herdianita, N.R., Browne, P.R.L., Rodgers, K.A. and Campbell, K.A. 2000. Mineralogical and textural changes accompanying ageing of silica sinter. *Mineralium Deposita* 35, pp. 48–62, DOI: 10.1007/s001260050005.

Irfan et al. 2021 – Irfan, U., Maulana, A. and Muhammad, F. 2021. Role of bedrock serpentinization on the development of nickel laterite deposit in Sorowako, Sulawesi, Indonesia. *IOP Conference Series: Earth and Environmental Science* 921, DOI: 10.1088/1755-1315/921/1/012028.

Kadarusman et al. 2004 – Kadarusman, A., Miyashita, S., Maruyama, S., Parkinson, C.D. and Ishikawa, A. 2004. Petrology, geochemistry and paleogeographic reconstruction of the East Sulawesi Ophiolite, Indonesia. *Tectonophysics* 392, pp. 55–83, DOI: 10.1016/J.TECTO.2004.04.008.

Klein et al. 2015 – Klein, F., Grozeva, N.G., Seewald, J.S., McCollom, T.M., Humphris, S.E., Moskowitz, B., Berquó, T.S. and Kahl, W.A. 2015. Experimental constraints on fluid-rock reactions during incipient serpentinization of harzburgite. *American Mineralogist* 100, pp. 991–1002, DOI: 10.2138/AM-2015-5112.

Konopka et al. 2022 – Konopka, G., Szamałek, K. and Zglinicki, K. 2022. Ni-Co Bearing Laterites from Halmahera Island (Indonesia). *Applied Sciences* 12(15), DOI: 10.3390/APP12157586.

Lamadrid et al. 2017 – Lamadrid, H.M., Rimstidt, J.D., Schwarzenbach, E.M., Klein, F., Ulrich, S., Dolocan, A. and Bodnar, R.J. 2017. Effect of water activity on rates of serpentinization of olivine. *Nature Communications* 8, pp. 1–9, DOI: 10.1038/ncomms16107.

Malvoisin et al. 2012 – Malvoisin, B., Brunet, F., Carlut, J., Rouméjon, S. and Cannat, M. 2012. Serpentinization of oceanic peridotites: 2. Kinetics and processes of San Carlos olivine hydrothermal alteration. *Journal of Geophysical Research: Solid Earth* 117, DOI: 10.1029/2011JB008842.

Marker et al. 1991 – Marker, A., Friedrich, G., Carvalho, A. and Melfi, A. 1991. Control of the distribution of Mn, Co, Zn, Zr, Ti and REEs during the evolution of lateritic covers above ultramafic complexes. *Journal of Geochemical Exploration* 40, pp. 361–383, DOI: 10.1016/0375-6742(91)90048-Y.

Martin, B. and Fyfe, W.S. 1970. Some experimental and theoretical observations on the kinetics of hydration reactions with particular reference to serpentinization. *Chemical Geology* 6, pp. 185–202, DOI: 10.1016/0009-2541(70)90018-5.

Mével, C. 2003. Serpentinisation of abyssal peridotite at mid ocean ridges. *Comptes Rendus Geoscience* 335, pp. 825–852, DOI: 10.1016/j.crte.2003.08.006.

Monnier et al. 1995 – Monnier, C., Girardeau, J., Maury, R. and Cotton, J. 1995. Back-arc basin origin for the East Sulawesi ophiolite (eastern Indonesia). *Geology* 23, pp. 851–854, DOI: 10.1130/0091-7613(1995)023<0851:BABOFT>2.3.CO;2.

Myagkiy et al. 2017 – Myagkiy, A., Truche, L., Cathelineau, M. and Golfier, F. 2017. Revealing the conditions of Ni mineralization in the laterite profiles of New Caledonia: Insights from reactive geochemical transport modelling. *Chemical Geology* 466, pp. 274–284, DOI: 10.1016/J.CHEMGEO.2017.06.018.

Pagé, P. and Barnes, S.J. 2009. Using Trace Elements in Chromites to Constrain the Origin of Podiform Chromitites in the Thetford Mines Ophiolite, Québec, Canada. *Economic Geology* 104, pp. 997–1018, DOI: 10.2113/ECONGEO.104.7.997.

Pagé et al. 2012 – Pagé, P., Barnes, S.J., Bédard, J.H. and Zientek, M.L. 2012. In situ determination of Os, Ir, and Ru in chromites formed from komatiite, tholeiite, and boninite magmas: Implications for chromite control of Os, Ir, and Ru during partial melting and crystal fractionation. *Chemical Geology* 302–303, pp. 3–15, DOI: 10.1016/J.CHEMGEO.2011.06.006.

Parkinson, C. 1998. Emplacement of the East Sulawesi Ophiolite: evidence from subophiolite metamorphic rocks. *Journal of Asian Earth Sciences* 16, pp. 13–28, DOI: 10.1016/S0743-9547(97)00039-1.

Pelletier, B. 1996. Serpentines in nickel silicate ore from New Caledonia. *Australasian Institute of Mining and Metallurgy Publication Series – Nickel Conference* 6, pp. 197–205.

Quantin et al. 2002 – Quantin, C., Becquer, T. and Berthelin, J. 2002. Mn-oxide: a major source of easily mobilisable Co and Ni under reducing conditions in New Caledonia Ferralsols. *Comptes Rendus Geoscience* 334, pp. 273–278, DOI: 10.1016/S1631-0713(02)01753-4.

Roqué-Rosell et al. 2010 – Roqué-Rosell, J., Mosselmans, J.F.W., Proenza, J.A., Labrador, M., Galí, S., Atkinson, K.D. and Quinn, P.D. 2010. Sorption of Ni by "lithiophorite–asbolane" intermediates in Moa Bay lateritic deposits, eastern Cuba. *Chemical Geology* 275, pp. 9–18, DOI: 10.1016/J.CHEMGEO.2010.04.006.

Santoro et al. 2022 – Santoro, L., Putzolu, F., Mondillo, N., Boni, M. and Herrington, R. 2022. Trace element geochemistry of iron-(oxy)-hydroxides in Ni(Co)-laterites: Review, new data and implications for ore forming processes. *Ore Geology Reviews* 140, DOI: 10.1016/J.OREGEOREV.2021.104501.

Schellmann, W. 1994. Geochemical differentiation in laterite and bauxite formation. *CATENA* 21, pp. 131–143, DOI: 10.1016/0341-8162(94)90007-8.

Schwertmann, U. and Murad, E. 1983. Effect of pH on the formation of goethite and hematite from ferrihydrite. *Clays and Clay Minerals* 31(4), pp. 277–284, DOI: 10.1346/CCMN.1983.0310405.

Schwertmann, U. and Taylor, R.M. 1989. *Iron oxides*. [In:] Dixon, J.B. and Weed, S.B. (eds.), *Minerals in Soil Environments*. Soil Science Society of America, Madison, Wis. pp. 379–438.

Singh et al. 2002 – Singh, B., Sherman, D.M., Gilkes, R.J., Wells, M.A. and Mosselmans, J.F.W. 2002. Incorporation of Cr, Mn and Ni into goethite (α-FeOOH): mechanism from extended X-ray absorption fine structure spectroscopy. *Clay Minerals* 37, pp. 639–649, DOI: 10.1180/00985502374066.

Soh Tamehe et al. 2024 – Soh Tamehe, L., Zhao, Y., Xu, W. and Gao, J. 2024. Ni(Co) Laterite Deposits of Southeast Asia: A Review and Perspective. *Minerals* 14(2), DOI: 10.3390/MIN14020134.

Streckeisen, A.L. 1973. Plutonic rocks, classification and nomenclature recommended by the IUGS subcommission on the systematics of igneous rocks. *Geotimes* 18, pp. 26–30.

Staude et al. 2023 – Staude, S., Scharrer, M., Markl, G., Simon, I., Pfaff, K., Monecke, T. and Blanc, P. 2023. Hydrothermal Pentlandite (Ni,Fe)9S8 from Kambalda, Western Australia: Occurrences, Formation Conditions, and Association with Orogenic Gold. *The Canadian Journal of Mineralogy and Petrology* 61, pp. 239–271, DOI: 10.3749/2200032.

Tauler et al. 2017 – Tauler, E., Lewis, J.F., Villanova-de-Benavent, C., Aiglsperger, T., Proenza, J.A., Domènech, C., Gallardo, T., Longo, F. and Galí, S. 2017. Discovery of Ni-smectite-rich saprolite at Loma Ortega, Falcondo mining district (Dominican Republic): geochemistry and mineralogy of an unusual case of "hybrid hydrous Mg silicate – clay silicate" type Ni-laterite. *Mineralium Deposita* 52, pp. 1011–1030, DOI: 10.1007/s00126-017-0750-8.

Thorne et al. 2009 – Thorne, R., Herrington, R. and Roberts, S. 2009. Composition and origin of the Çaldağ oxide nickel laterite, W. Turkey. *Mineralium Deposita* 44, pp. 581–595, DOI: 10.1007/S00126-009-0234-6.

Ulrich et al. 2019 – Ulrich, M., Cathelineau, M., Muñoz, M., Boiron, M.C., Teitler, Y. and Karpoff, A.M. 2019. The relative distribution of critical (Sc, REE) and transition metals (Ni, Co, Cr, Mn, V) in some Ni-laterite deposits of New Caledonia. *Journal of Geochemical Exploration* 197, pp. 93–113, DOI: 10.1016/J.GEXPLO.2018.11.017.

Villanova-de-Benavent et al. 2014 – Villanova-de-Benavent, C., Proenza, J. A., Galí, S., García-Casco, A., Tauler, E., Lewis, J.F. and Longo, F. 2014. Garnierites and garnierites: Textures, mineralogy and geochemistry of garnierites in the Falcondo Ni-laterite deposit, Dominican Republic. *Ore Geology Reviews* 58, pp. 91–109, DOI: 10.1016/J.OREGEOREV.2013.10.008.

Villanova-de-Benavent et al. 2019 – Villanova-de-Benavent, C., Jawhari, T., Roqué-Rosell, J., Galí, S. and Proenza, J.A. 2019. Ni-bearing phyllosilicates ("garnierites"): New insights from thermal analysis, μRaman and IR spectroscopy. *Applied Clay Science* 175, pp. 47–66, DOI: 10.1016/J.CLAY.2019.03.036.

Wegner, W.W. and Ernst, W.G. 1983, Experimentally determined hydration and dehydration reaction rates in the system MgO-SiO_2-H_2O, *American Journal of Science* 283, pp. 151–180.

Wells et al. 2022 – Wells, M.A., Ramanaidou, E.R., Zakaria Quadir, M., Roberts, M., Bourdet, J. and Verrall, M. 2022. Morphology, composition and dissolution of chromite in the Goro lateritic nickel deposit, New Caledonia: Insight into ophiolite and laterite genesis. *Ore Geology Reviews* 143, DOI: 10.1016/J.OREGEOREV.2022.104752.

White et al. 2014 – White, L.T., Hall, R. and Armstrong, R.A. 2014. The age of undeformed dacite intrusions within the Kolaka Fault zone, SE Sulawesi, Indonesia. *Journal of Asian Earth Sciences* 94, pp. 105–112, DOI: 10.1016/J.JSEAES.2014.08.014.

Wulandari et al. 2020 – Wulandari, W., Kinda, M.M., Murida, R. and Samadhi, T.W. 2020. The Effect of Alkali Roasting Pretreatment on Nickel Extraction from Limonite Ore by Using Dissolved SO_2-Air. *Minerals* 10, pp. 701–713, DOI: 10.3390/MIN10080701.

Zhang et al. 2020 – Zhang, Y., Qie, J., Wang, X. F., Cui, K., Fu, T., Wang, J. and Qi, Y. 2020. Mineralogical Characteristics of the Nickel Laterite, Southeast Ophiolite Belt, Sulawesi Island, Indonesia. *Mining, Metallurgy and Exploration* 37, pp. 79–91, DOI: 10.1007/S42461-019-00147-Y.

THE CHARACTERISTICS OF SAPROLITIC NICKEL ORE FROM LATERITIC NICKEL DEPOSIT IN THE MANDIODO AREA, NORTH KONAWE, INDONESIA

Keywords

weathering, Lateritic nickel deposit, bedrock, saprolite, serpentinization

Abstract

The study of saprolitic nickel ore conducted in the Mandiodo area of North Konawe, Indonesia, reveals a high nickel content. Mineralogical and geochemical analyses from bedrock to saprolite horizon samples reveal the characteristics of the ore as a weathering product from the peridotite bedrock composed mainly of olivine, pyroxene, and serpentine. The results reveal an advanced serpentinization process, indicated by the domination of olivine and serpentine, represented by forsterite and chrysotile, respectively, with a lower amount of enstatite, a member of the pyroxene group, in the bedrock. Further, the abundance of goethite, amphibole, and chlorite mineral groups in the saprock and saprolite indicate an initial stage of weathering. After the weathering of the bedrock, the serpentine is the primary source of Ni in the saprock and saprolite horizon, with a minor occurrence in goethite. Pentlandite is rarely present in the bedrock but is often found with a very high Ni content. In the saprolite ore, the content of Ni hosted by serpentine-group minerals and Fe from goethite increased drastically up to 4.6 and 43.8 wt%, respectively, followed by the drastic depletion of Si and Mg to 7.3 and 3.9 wt%, respectively. The presence of chromite in the saprolite horizon plays a significant role during the enrichment of Cr and Al, and the Mn is hosted by both Mn-oxides and goethite. Geochemical variations in the saprolitic horizon indicate the prospect of future critical metal resources in the study area.

CHARAKTERYSTYKA RUDY NIKLU SAPROLITYCZNEGO Z LATERYTOWEGO ZŁOŻA NIKLU W REJONIE MANDIODO, NORTH KONAWE, INDONEZJA

Słowa kluczowe

wietrzenie, laterytowe złoże niklu, podłoże skalne, saprolit, serpentynizacja

Streszczenie

Badanie rudy niklu saprolitycznego przeprowadzone w rejonie Mandiodo w Okręgu Północnym Konawe w Indonezji wykazało wysoką zawartość niklu. Analizy mineralogiczne i geochemiczne od podłoża skalnego do próbek horyzontu saprolitu ujawniają cechy rudy jako produktu wietrzenia z podłoża perydotytowego składającego się głównie z oliwinu, piroksenu i serpentynu. Wyniki ujawniają zaawansowany proces serpentynizacji, na który wskazuje dominacja oliwinu i serpentynu reprezentowanych odpowiednio przez forsteryt i chryzotyl, z mniejszą ilością enstatytu jako członka grupy piroksenów w podłożu skalnym. Ponadto obfitość grup mineralnych goethytu, amfibolu i chlorytu w saprocie i saprolicie wskazuje na początkowy etap wietrzenia. Po zwietrzeniu podłoża

skalnego serpentynit jest głównym źródłem Ni w poziomie saproku i saprolitu, z niewielkim występowaniem w goethycie. Pentlandyt rzadko występuje w podłożu skalnym, ale pojawia się z bardzo wysoką zawartością Ni. W rudzie saprolitu zawartość Ni w minerałach grupy serpentynu i Fe w goethycie wzrosła drastycznie do odpowiednio 4,6 i 43,8% wag., po czym nastąpiło drastyczne wyczerpanie Si i Mg do odpowiednio 7,3 i 3,9% wag. Obecność chromitu w poziomie saprolitu odgrywa znaczącą rolę podczas wzbogacania Cr i Al, a Mn jest obecny zarówno w tlenkach Mn, jak i w goethycie. Zmiany geochemiczne w poziomie saprolitu wskazują na perspektywę przyszłych zasobów metali krytycznych w badanym obszarze.